



Published in final edited form as:

*J Med Chem.* 2020 September 10; 63(17): 9512–9522. doi:10.1021/acs.jmedchem.0c00689.

## Selective Peptidomimetic Inhibitors of NTMT1/2: Rational design, synthesis, characterization, and crystallographic studies

Brianna D. Mackie<sup>†</sup>, Dongxing Chen<sup>‡</sup>, Guangping Dong<sup>‡</sup>, Cheng Dong<sup>¶</sup>, Haley Parker<sup>#</sup>, Christine E. Schaner Tooley<sup>#</sup>, Nicholas Noinaj<sup>§</sup>, Jinrong Min<sup>¶</sup>, Rong Huang<sup>\*,†,‡</sup>

<sup>†</sup> Department of Medicinal Chemistry, Institute of Structural Biology, Drug Discovery and Development, School of Pharmacy, Virginia Commonwealth University, Richmond, VA 23298, United States

<sup>‡</sup> Department of Medicinal Chemistry and Molecular Pharmacology, Purdue Institute for Drug Discovery, Purdue University Center for Cancer Research, Purdue University, West Lafayette, IN 47907, United States

<sup>¶</sup> Structural Genomics Consortium, Department of Physiology, University of Toronto, Toronto, Ontario, M5G 1L7 Canada.

<sup>#</sup> Department of Biochemistry, Jacobs School of Medicine and Biomedical Sciences, University at Buffalo, Buffalo, NY 14203, United States

<sup>§</sup> Department of Biological Sciences, Markey Center for Structural Biology, and the Purdue Institute of Inflammation, Immunology and Infectious Disease, Purdue University, West Lafayette, IN 47907, United States

### Abstract

Protein N-terminal methyltransferases (NTMTs) methylate the  $\alpha$ -N-terminal amines of proteins starting with the canonical X-P-K/R motif. Genetic studies imply that NTMT1 regulates cell mitosis and DNA damage repair. Herein, we report the rational design and development of the first potent peptidomimetic inhibitors for NTMT1/2. Biochemical and co-crystallization studies manifest that **BM30** (IC<sub>50</sub> of 0.89 ± 0.10  $\mu$ M) is a competitive inhibitor to the peptide substrate and noncompetitive to the cofactor S-adenosylmethionine. **BM30** exhibits over 100-fold selectivity to NTMT1/2 among a panel of 41 methyltransferases, indicating the potential to

\*Corresponding Author: Phone: (765) 494 3426. huang-r@purdue.edu.

#### Author Contributions

The manuscript was written through contributions of all authors. All authors have given approval to the final version of the manuscript.

The authors declare no competing financial interest.

#### ASSOCIATED CONTENT

##### Supporting Information

The Supporting Information is available free of charge on the ACS Publications website.

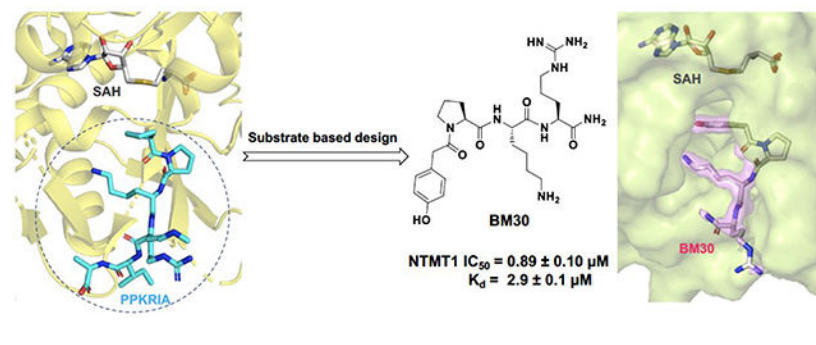
Figure S1. MALDI-MS and HPLC spectra of compounds **1-24**, **DC431** and **DC432**; Figure S2. IC<sub>50</sub> curve of compound **5**; Figure S3. IC<sub>50</sub> curve of **BM30**; Figure S4. Cell permeability evaluation; Table S1. Selectivity study **BM30** and **22** against G9a and PRMT1; Table S2. Selectivity study of **BM30** against a panel of 41 MTases (Reaction Biology); Table S3. Crystallography data and refinement statistics (PDB ID: 6WH8); Table S4. IC<sub>50</sub> values and binding affinities of **BM30** and its cell-permeable analogs. Molecular formula strings (CSV)

#### Accession Codes

The coordinates for the structure of human NTMT1 in complex with **BM30** have been deposited under PDB ID 6WH8. Authors will release the atomic coordinates and experimental data upon article publication.

achieve high selectivity when targeting the peptide substrate binding site of NTMT1/2. Its cell-permeable analog **DC432** ( $IC_{50}$  of  $54 \pm 4$  nM) decreases the N-terminal methylation level of regulator of chromosome condensation 1 and SET proteins in HCT116 cells. This proof-of-principle study provides valuable probes for NTMT1/2 and highlights the opportunity to develop more cell-potent inhibitors to elucidate the function of NTMTs in the future.

## Graphical Abstract



## INTRODUCTION

Protein methylation is an important epigenetic modification that regulates dynamic chromatin states and transcription.<sup>1,2</sup> Therefore, potent and specific inhibitors of protein methyltransferases can serve as valuable chemical probes to elucidate the function in physiological and pathological contexts. For example, recently approved Tazverik (tazemetostat) for epithelioid sarcoma treatment is an inhibitor for protein lysine methyltransferase (PKMT) EZH2. Another PKMT inhibitor, Pinometostat targeting DOT1L, is in a phase I trial for combination use for patients with acute myeloid leukemia.<sup>1</sup> In addition, a few protein arginine methyltransferase 5 (PRMT5) inhibitors, including JNJ64619178, GSK3326595, PF06939999, and PRT811, are also in clinical trials for advanced solid tumors.<sup>3</sup>

Protein  $\alpha$ -N-terminal methylation has been known for nearly four decades since it was first uncovered on bacteria ribosomal proteins L33.<sup>4,5</sup> The identification of N-terminal methyltransferase 1 (NTMT1/NRMT1) unveiled the first methylation writer for human protein  $\alpha$ -N-termini.<sup>6,7</sup> In addition to NTMT1, its close homolog NTMT2/NRMT2 that shares over 50% sequence similarity has been identified as another writer for human protein  $\alpha$ -N-terminal methylation.<sup>8</sup> Both NTMT1 and 2 share the same X-P-K/R canonical recognition motif, where X can be any amino acid although D and E are not preferred.<sup>9-11</sup> Recently, METTL13 has been discovered to solely methylate the elongation factor 1A (EF1A) on both the  $\alpha$ -N-terminus and lysine side chain.<sup>12,13</sup> However, the N-terminal sequence of EF1A is different from the X-P-K/R motif that NTMT1/2 prefer. Structural studies on NTMT1/2 in complex with their substrate peptides reveal that the peptide substrates bind at a defined binding pocket that juxtapose with the cofactor S-adenosyl methionine (SAM) binding site.<sup>9-11</sup> This is distinct from PKMTs and PRMTs, which normally have a narrow channel to accommodate only the side chain of the Lys or Arg. The

structural information gained from the co-crystal structures substantiated the unique substrate selectivity of NTMT1/2.<sup>9–11</sup>

Protein  $\alpha$ -N-terminal methylation was originally proposed to regulate protein-protein interactions since the methylated proteins initially identified were involved in large macromolecular complexes including histone proteins, cytochrome c-557, and myosin light chain proteins.<sup>4,14</sup> Recent discoveries have demonstrated its relevance in protein-DNA interactions, as shown in strengthening the interactions of chromatin with centromere protein A (CENPA) and regulator of chromosome condensation 1 (RCC1), as well as DNA damage-binding protein 2 (DDB2) to DNA damage foci.<sup>15–17</sup> Meanwhile, newly identified substrates of NTMT1 also include the tumor suppressor retinoblastoma 1 (RB1), oncoprotein SET, and poly(ADP-ribose) polymerase 3.<sup>6,18</sup> In addition, previous genetic studies have inferred the importance of NTMT1 in mitosis, DNA damage repair, aging, and a variety of cancers.<sup>6,16,17,19–21</sup> Despite the aforementioned progresses, our understanding of protein  $\alpha$ -N-terminal methylation function is still in its infancy. Therefore, it is imperative to discover specific and potent inhibitors for NTMTs to probe their biological functions. Guided by the kinetic mechanism of NTMT1, bisubstrate analogs that covalently link both SAM and peptide substrate were designed to mimic the transition state and displayed high selectivity and potency for NTMT1.<sup>22–26</sup> Nevertheless, intrinsic properties of those bisubstrate analogs impose a challenge to penetrate cell membranes, which limit their applications in cell-based studies. Therefore, there is a need for a new strategy to discover inhibitors for NTMTs in order to probe the downstream process of protein  $\alpha$ -N-terminal methylation. Given that the NTMT family has a unique peptide substrate binding site, we hypothesize that targeting the peptide binding site should achieve higher selectivity for NTMTs. Herein, we report the design and synthesis of the first potent and selective peptidomimetic inhibitors for the NTMT1/2.

## RESULTS AND DISCUSSION

### Design

According to the crystal structures of NTMT1 in complex with peptide substrates (XPKRIA), the backbone carbonyl group of the first amino acid (X1) interacts with a conserved Asn168 residue NTMT1 through H-bonding.<sup>9,27</sup> Mutation of Asn168 to Lys resulted in a ~36-fold loss in  $K_m$ , indicating the importance of this interaction between NTMT1 and its peptide substrate<sup>9</sup>. However, the tolerance at the first position of the substrate suggests a possible spacious binding pocket surrounding the first position. The N-terminal amine of the peptide substrate points toward the methyl group of the SAM and serves as a nucleophile to receive the methyl group from the SAM. The second residue P2 forms a stacking interaction with the indole of Trp136. The third residue K3 forms two key hydrogen bonds with side chains of two aspartic acids.<sup>9–11</sup> Either a Lys or Arg residue has been discovered at the third position of known protein substrates. The fourth amino acid is adjacent to a negatively charged substrate binding channel, where the fifth and sixth residues are primarily exposed to the solvent.<sup>9–11</sup> Hence, we speculate that the  $\alpha$ -N-terminal amine is essential for methyl transfer by acting as a nucleophile to attack SAM, but it is not essential for binding. Therefore, we hypothesized that the removal of the N-terminal amine of

NTMT1/2 peptide substrates would convert the substrate into an inhibitor. Since the first four amino acids contribute significantly to the interaction with NTMT1/2, we initiated our efforts by incorporating different substitutions (**R**<sub>1</sub>) onto a tripeptide (PKR) through an amid bond (Figure 1) to retain as much interaction as the peptide substrates. PPKRIA and YPKRIA are two peptide substrates for NTMT1 with a  $K_d$  value at  $0.7 \pm 0.2$  nM and  $0.1 \pm 0.08$   $\mu$ M, respectively.<sup>9</sup> Hence, compounds **1-5** were designed to mimic the Pro or Tyr moiety by introducing cyclopentane, cyclohexane, furan, phenyl, and a benzyl moiety as the **R**<sub>1</sub> group.

## Synthesis

The peptides were synthesized following the standard Fmoc solid-phase synthesis on Rink amide resin using a CEM Liberty microwave peptide synthesizer. The peptidomimetics that have carboxylic acids at the first position were prepared through the standard amino acid coupling reaction (Scheme 1). All compounds were cleaved from the solid support in a cleavage cocktail consisting of trifluoroacetic acid/2,2'-(ethylenedioxy)diethanethiol/H<sub>2</sub>O/triisopropylsilane (94:2.5:2.5:1), and followed by purification through reverse-phase HPLC and characterized through mass spectrometry (Figure S1).

## Biochemical Characterization

All peptidomimetics were first subject to a methylation progression MALDI-MS study to examine if they were NTMT1 substrates.<sup>22,28</sup> None of the peptidomimetics displayed any methylation, indicating that they were not NTMT1 substrates. Next, the synthesized peptidomimetics were evaluated in a SAH hydrolase (SAHH)-coupled fluorescence assay at 100  $\mu$ M of SAM and at the  $K_m$  value of the peptide substrate (SPKRIA or GPKRIA).<sup>22</sup> Initial screening was carried out at the concentration of 5  $\mu$ M, 30  $\mu$ M, and 100  $\mu$ M of each compound. Compound **5** exhibited more than 50% of inhibition at 30  $\mu$ M, and was then subjected to subsequent IC<sub>50</sub> studies by ranging the inhibitor concentration from 0 – 100  $\mu$ M in a three-fold dilution. Compound **5** showed an IC<sub>50</sub> of  $6.85 \pm 2.82$   $\mu$ M (Figure S2). A summary of the IC<sub>50</sub> values for the peptidomimetics is shown in Table 1.

## Structure-Activity Relationship (SAR) Studies

In order to improve the inhibitory activity of the peptidomimetics, SAR studies were conducted by using **5** as the lead compound (Tables 1–2).

**The first (**R**<sub>1</sub>) position**—The benzoyl substitution of compound **5** resembled the side chain of Tyr; therefore, we focused our SAR investigation on introducing various para-substitutions on the phenyl ring, including a hydroxy, an amino, and a methoxy group at the para-position of the phenyl ring to yield compounds **6-8** (Table 1). Among all synthesized peptidomimetics, compound **6 (BM30)** which contained a hydroxyl group at the para position showed the greatest inhibitory activity with an IC<sub>50</sub> of  $0.89 \pm 0.10$   $\mu$ M (Figure S3), approximately 7-fold increased activity compared to **5**. However, a methoxy substitution led to a loss of inhibition of **8** (IC<sub>50</sub> > 100  $\mu$ M), while its constitutional isomer **9** rescued the inhibitory activity (IC<sub>50</sub> =  $1.5 \pm 0.1$   $\mu$ M) with a 4-hydroxymethyl substitution. This suggests the preference of a H-bond donor at the first position. Given that introducing a methylene

linker between the phenyl ring and the carbonyl group significantly increased the inhibition of **5** compared to **4**, an ethylene linker was introduced in **10** and **11** to probe the optimal linker length (Table 1). Both **10** and **11** displayed a 5-fold and 3-fold loss in inhibition compared to their respective parent compounds **6** and **7**, suggesting a methylene group as the optimal linker for the NTMT1 inhibitor. Lastly, compound **12** was prepared to explore the importance of the carbonyl group at the first position. Nevertheless, **12** did not show any inhibitory activity at 100  $\mu$ M, implying the significance of the carbonyl group at the first position.

**The second position**—All available co-crystal structures of NTMT1/2 in complex with X-P-K/R substrates reveal that Pro2 only exhibits the trans conformation, suggesting that the trans conformation is favored to interact with NTMT1/2.<sup>9,11,27</sup> To verify the preference of this trans-conformation, an alpha-methyl-Pro was introduced at the 2nd position since the predominant conformation of alpha-methyl-Pro is cis.<sup>29</sup> The resulting compound **13** completely lost the inhibitory activity for NTMT1 (Table 2). These results substantiate previous findings that the Pro2 prefers the trans conformation; however, the additional methyl group may also introduce certain steric hindrances. Next, ortho- and meta-amino benzoic acids were also introduced at Pro2 to generate **14** and **15**, respectively. Both compounds did not exhibit any inhibitory activity, denoting the importance of Pro2 in the canonical X-P-K/R motif. *The 3<sup>rd</sup> and 4<sup>th</sup> position.* Next, we explored the modifications at the third and fourth position in an attempt to increase inhibitory activity, as well as to enhance stability since peptide-based inhibitors are susceptible to degradation (Table 2). Arg has been detected at the 3rd position in the validated NTMT1 substrate CENP-A (GPRR),<sup>10,15</sup> thus **16** was synthesized with Arg at the 3<sup>rd</sup> position. However, **16** displayed over a 20-fold loss of inhibition compared to **6**. This result signified the preference for Lys over Arg at the third position, potentially due to its important role in interacting with two acidic residues (Asp177 and Asp180 in NTMT1; Asp232 and Asp 235 in NTMT2).<sup>9–11</sup> Although Arg and Lys are two prevalent amino acids at the 4<sup>th</sup> position of the NTMT1 substrate peptides, additional amino acids have been observed in reported NTMT1 substrates. Therefore, Lys, Thr, Ala, and Gly were introduced to replace the Arg at the 4<sup>th</sup> position of **BM30** to generate **17-21** to examine the contribution of side chain at this position because it is pointed to the solvent in the co-crystal structures.<sup>9</sup> Compound **17**, which included a Lys in the 4<sup>th</sup> position, exhibited negligible difference in inhibition compared to **BM30** which contains an Arg. Introducing Thr or Ala at the 4<sup>th</sup> position led to a 5-fold of loss as shown in **18-19**, while incorporating Gly produced almost a 14-fold loss in inhibition as shown in **20**. When the 4<sup>th</sup> position was eliminated to yield **21**, inhibitory activity decreased 18-fold compared to **BM30**. The result indicated that the side chain of the 4<sup>th</sup> amino acid does contribute to the NTMT1 interaction although it points towards to the solvent in the co-crystal structures. Additionally, non-natural amino acid was also made at either the 3<sup>rd</sup> or 4<sup>th</sup> position to produce **22-24** in attempts to increase the stability against proteases. However, loss of inhibition ranging from nearly 5- to 37-fold was observed in compounds **22-24** compared to **BM30**, although **22** was the most potent one among these three protease-stable analogues.

## Selectivity Studies

Given that many methyltransferases exist, selectivity of the inhibitor is a critical requirement for its potential as a valuable probe. We first investigated the selectivity of **BM30** and **22** against one representative member from the protein lysine methyltransferase PKMT (G9a) and protein arginine methyltransferase PRMT (PRMT1) families. Both enzymes share a cofactor SAM binding site despite having different substrate peptide binding sites from NTMT1. As shown in Table S1, **BM30** demonstrated >100  $\mu\text{M}$   $\text{IC}_{50}$  values against both G9a and PRMT1, but **22** also exhibited inhibition for G9a. Thus, we proceeded with **BM30** to evaluate its selectivity against a panel of 41 MTases (Reaction Biology) that include NTMT1/2, PKMTs, PRMTs, and DNMTs (Figure 2, Table S2). The results indicated that **BM30** displays comparable inhibition against both NTMT1 and NTMT2, which was not surprising since NTMT1/2 share the canonical X-P-K/R recognition motif. Strikingly, **BM30** exhibited very marginal inhibition against the remaining 39 MTases even at 100  $\mu\text{M}$ . The over 100-fold selectivity that **BM30** displays for NTMT1/2 compared to PKMTs, PRMTs, and DNMTs evinces the unique substrate specificity of NTMT1/2.

## Inhibition Mechanism

Kinetic characterization of **BM30** was performed to examine its mechanism of action using the SAHH-coupled fluorescence-based assay (Figure 3). As shown in Figure 3, **BM30** exhibited a competitive inhibition pattern with respect to the NTMT1 peptide substrate RCC1–6 (SPKRIA). This is demonstrated by an ascending and linear dependence of the  $\text{IC}_{50}$  values relative to the increasing peptide substrate concentration of RCC1–6. On the other hand, **BM30** displayed a noncompetitive inhibition pattern with respect to the cofactor SAM, indicated by a line that is parallel to the x-axis. These results verify that **BM30** competitively binds to the peptide substrate binding site, supporting our design strategy.

## Crystal Structure of the NTMT1-BM30-SAH Complex

To further confirm that **BM30** binds to the peptide substrate binding site of NTMT1, we solved the X-ray co-crystal structure of NTMT1-**BM30**-SAH (PDB ID: 6WH8) (Figure 4A–C). **BM30** occupies the peptide substrate binding site of NTMT1. Superimposition of our NTMT1-**BM30**-SAH structure with the published NTMT1-YPKRIA-SAH ternary complex (PDB ID: 5E1D) gave an RMSD value of 0.12 Å (across all residues of chain A, Figure 4D–E). The **BM30**-NTMT1 complex retains the same interactions as previously observed with YPKRIA-NTMT1 in the ternary complex of substrate peptide/SAH.<sup>9</sup> For instance, the carbonyl oxygen of the 4-hydroxyl phenyl acetic acid interacts with the side chain of Asn168 through hydrogen bonding. The second Pro occupies a hydrophobic pocket that is formed by Leu31, Ile37, and Ile214. In addition, the  $\epsilon$ -amine of the third Lys forms electronic interactions with carboxylate groups of Asp177 and Asp180. In addition, a direct H-bond exists between the carbonyl oxygen of the fourth Arg and Try215. The 4-hydroxyl group of the phenyl ring also forms a H-bond with Asp180 and one water molecule.

## Design and characterization of DC431 and DC432

We tested the cell permeability of **BM30** through MS detection of its cellular levels.<sup>30</sup> However, **BM30** was minimally detected at 100  $\mu\text{M}$  inside the cells (Figure S4). In order to

increase the cell permeability, we designed and synthesized **DC431** and **DC432** by attaching cell-permeable peptide TAT (GRKKRRQRRR-NH<sub>2</sub>) and five Arg at the C-terminus of **BM30**, respectively. It is known that incorporating six Arg into compounds can increase the cell-permeability.<sup>31</sup> Hence, five additional Arg were added to **BM30** to generate **DC432** because **BM30** already had one Arg at its C-terminus. Given that the first four amino acids contribute significantly to the binding for NTMT1/2, we hypothesized that **DC431** and **DC432** would have slightly increased inhibitory activities than **BM30**, since they contained additional amino acids at the C-terminus of **BM30**. To confirm our hypothesis, IC<sub>50</sub> values of **DC431** and **DC432** were determined to be 0.23±0.03 μM and 0.054±0.004 μM, respectively (Figure 5A&B). **DC431** demonstrated a 4-fold increased inhibition for NTMT1 than **BM30** as predicted. Surprisingly, **DC432** displayed a 4-fold higher activity than **DC431** and 16-fold inhibitory activity compared to **BM30**.

In addition, we tested the levels of N-terminal methylation by directly incubating the inhibitors with NTMT1, SAM and full-length substrate protein RCC1. At 2 μM of **BM30** or **DC432**, there is a slight increase of me2-RCC1 levels and decrease of me3-RCC1 levels as compared to untreated samples (Figure 5C). An increase in me2-RCC1 levels indicates inhibition of NTMT1 trimethylation, as NTMT1 is a distributive enzyme that normally reaches saturated trimethylation levels under these conditions.<sup>22</sup> The appearance and persistence of me2-RCC1 signals enzymatic inhibition. At 10 and 50 μM, there was a considerable decrease in me3-RCC1 levels and increase in me2-RCC1 levels for all three inhibitors (Figure 5C). To further validate their interactions with both NTMT1 and 2, we determined binding affinities of both cell-permeable analogs and **BM30** via isothermal titration calorimetry (Figure 6A&B, Table S4). **BM30** exhibited a comparable K<sub>d</sub> value of 3.0 μM and 3.7 μM to NTMT1 and 2, respectively. But **DC431** showed a 4-fold increase in binding to NTMT1. Furthermore, **DC432** displayed an 8-fold and 4-fold tighter binding affinity to NTMT1 and NTMT2, respectively. Increased inhibitory activities and binding affinities of both **DC431** and **DC432** corroborated the contributing roles of C-terminal amino acids to XPKR, as demonstrated before in the NTMT1-SPKRIA-SAH and NTMT2-SPKRIA-SAH ternary complexes.<sup>9,11</sup> In addition, there is 3- to 6-fold difference in **DC431** and **DC432** for NTMT1 over NTMT2 based on the data from ITC, but unmodified **BM30** showed similar K<sub>d</sub> values in both NTMT1/2. This change of the selectivity for NTMT1/2 demonstrated the contribution of C-terminal sequence to the selectivity, suggesting the potential of development of selective inhibitors for NTMT1 over its homolog NTMT2. Furthermore, enhanced cell penetration of **DC431** and **DC432** were also confirmed through a cellular MS assay. Both **DC431** and **DC432** exhibited cellular penetration even at 1 μM, while **BM30** did not display any even at 100 μM (Figure S4).

### Cellular N-terminal Methylation Level

NTMT1 can catalyze the trimethylation of its substrate starting with an SPK motif. Therefore, a cell permeable inhibitor of NTMT1 would be expected to decrease this trimethylation level. Then we proceeded to assess the inhibitory effects of **DC432** on the N-terminal trimethylation level via western blotting with a specific antibody to the N-terminal me3-SPK motif. As shown in Figure 7, treatment with **DC432** for 72 h in HCT116 cells did result in a decrease in the me3-SPK level at 100 μM. Although the impact on mono- and di-

methylation levels were not examined for this investigation, cellular inhibition was over 100-fold lower than the value obtained from the enzymatic assay (Figure 5B). The discrepancy between these results may be due to low efficiency of **DC432** to reach the target since NTMT1 is predominantly in the nucleus as reported before.<sup>6,8,27</sup>

## CONCLUSION

In summary, this study describes the discovery of the first potent and selective peptidomimetic inhibitor **BM30** for NTMT1/2 reported to date. Furthermore, **BM30** exhibits over 100-fold selectively against NTMT1/2 among a panel of 41 MTases. The cell-permeable derivative **DC432** represses N-terminal methylation levels of NTMT1/2 substrates in HCT116 cells, demonstrating that **DC432** would be a valuable probe for mechanistic studies of NTMT1/2 in cellular contexts. In addition, the crystal structure of **BM30** in complex with NTMT1 revealed the structural basis for its potency and selectivity, which paves the way for the future design and development of inhibitors with improved cell potency.

## MATERIALS AND METHODS

### Chemistry General Information

All reagents and solvents were purchased from commercial sources (Fisher, Aldrich, and Chem-Impex) and used directly. Final compounds were purified on preparative high-pressure liquid chromatography (RP-HPLC) was performed on either Waters 1525 or Agilent 1260 Series system. Systems were run with 0–20% methanol/water gradient with 0.1% TFA. Matrix-assisted laser desorption ionization mass spectra (MALDI-MS) data were acquired in positive-ion mode using a Sciex 4800 MALDI TOF/TOF MS. The peptides (PKR, PKRIA and PRRRS) were synthesized on a CEM Liberty Blue Automated Microwave Peptide Synthesizer with the manufacturers standard coupling cycles at 0.1 mmol scale. All compounds were cleaved from the resin in a cocktail of trifluoroacetic acid/2,2'-(ethylenedioxy)diethanethiol/H<sub>2</sub>O/trisopropylsilane (94:2.5:2.5:1) and confirmed by mass spectrometry. The purity of final compounds was confirmed through Agilent 1260 Series HPLC system by running with 5% to 30% methanol/water gradient with 0.1% TFA. All the purity of target compounds showed >95%.

### Cell Culture and Antibodies

HCT116 cells were obtained from ATCC and were cultured in McCoy's 5A (modified) medium (Gibco, #16600082), supplemented with 10% FBS (Gibco, #16000044) and 1% antibiotic-antimycotic (Gibco, #15240062). Antibodies against following proteins were used: Me3-SPK (Schaner Tooley lab <sup>6</sup>), RCC1 (Proteintech, #22142-1-AP), SET (Proteintech, #55201-1-AP), Lamin B1 (Proteintech, # 12987-1-AP), Anti-rabbit IgG, HRP-linked (Cell Signaling, #7074S).

### NTMT1 Biochemical Assays

Expression and purification of NTMT1 was performed as previously described.<sup>25</sup> Kinetic characterization of the peptide inhibitors was determined in a fluorescence-based SAHH-



coupled assay as described before. The inhibitors were added at concentrations ranging from 0 to 100  $\mu\text{M}$  following a three-fold dilution. The methylation assay was performed under the following conditions: 25 mM Tris (pH = 7.5), 50 mM KCl, 0.01% Triton X-100, 5  $\mu\text{M}$  SAHH, 0.2  $\mu\text{M}$  NTMT1, 100  $\mu\text{M}$  SAM, and 15  $\mu\text{M}$  ThioGlo1. After 10 min of incubation at 37  $^{\circ}\text{C}$ , the reaction was initiated with 10  $\mu\text{L}$  of 50  $\mu\text{M}$  RCC1–6 for a total volume of 100  $\mu\text{L}$ . Fluorescence intensity was monitored using a BMG ClarioStar microplate reader (Ex = 370 nm, Em=500 nm) at 37  $^{\circ}\text{C}$  for 15 min. The rates were fit to the log[inhibitor] vs response-variable slope (four parameters) model using least squares nonlinear regression using GraphPad Prism software 7 or 8. All experiments were performed in triplicate.

Inhibition Mechanism of BM30 was performed using the fluorescent-based assay described above. Six independent  $\text{IC}_{50}$  studies of BM30 were performed in triplicate with varying concentrations of substrate peptide, RCC1–6 and SAM at its  $K_m$  value. The inhibitors ranging in concentration (1  $\mu\text{L}$  of 0 – 10 mM) and following a three-fold dilution were incubated in the well-solution that was added in the following order: ddH<sub>2</sub>O, buffer (10  $\mu\text{L}$  of 250 mM Tris, pH 7.4 and 500 mM KCl), SAM (1  $\mu\text{L}$  of 10  $\mu\text{M}$ ), SAH hydrolase (5  $\mu\text{L}$  of 10 mg/mL), NTMT1 (0.5  $\mu\text{L}$  of 40  $\mu\text{M}$ ) and ThioGlo1 (1  $\mu\text{L}$  of 1.5 mM). After 10 min of incubation at 37  $^{\circ}\text{C}$ , the reaction was initiated with each concentration of RCC1–6 (10  $\mu\text{L}$  of 5, 10, 15, 20, 40, 80  $\mu\text{M}$ ) for a total volume of 100  $\mu\text{L}$ . The final concentrations are buffer (25 mM Tris, pH 7.4 and 50 mM KCl), SAM (1  $\mu\text{M}$ ), SAH hydrolase (10  $\mu\text{M}$ ), NTMT1 (0.2  $\mu\text{M}$ ), inhibitors (0 – 100  $\mu\text{M}$ ), RCC1–6 (0.25 $K_m$ , 0.5 $K_m$ , 0.75 $K_m$ ,  $K_m$ , 2 $K_m$ , and 4 $K_m$ , 0.5, 1, 1.5, 2, 4, 8  $\mu\text{M}$ , respectively) and Thioglo1 (15  $\mu\text{M}$ ). Fluorescence intensity was monitored using a CLARIOstar microplate reader (Ex = 370 nm, Em=500 nm) at 37  $^{\circ}\text{C}$  for 15 min. The rates were fit to the log[inhibitor] vs response model using least squares nonlinear regression through GraphPad Prism 7 software. The average  $\text{IC}_{50}$  value of each independent triplicate study was then plotted against the concentration of the [RCC1–6]/ $K_m$ . Next, the same experiment was repeated with six  $\text{IC}_{50}$  studies of BM30 in triplicate at varying concentrations of SAM (1  $\mu\text{L}$  of 31.25, 62.5, 125, 250, 500, and 1000  $\mu\text{M}$ ) and RCC1–6 at its  $K_m$  value. The final concentrations are buffer (25 mM Tris, pH 7.4 and 50 mM KCl), SAM (0.3125 $K_m$ , 0.625 $K_m$ , 1.25 $K_m$ , 2.5 $K_m$ , 5 $K_m$ , and 10 $K_m$ , 0.3125, 0.625, 1.25, 2.5, 5, 10  $\mu\text{M}$ , respectively), SAH hydrolase (10  $\mu\text{M}$ ), NTMT1 (0.2  $\mu\text{M}$ ), inhibitors (0 – 100  $\mu\text{M}$ ), RCC1–6 (2  $\mu\text{M}$ ) and Thioglo1 (15  $\mu\text{M}$ ). The average  $\text{IC}_{50}$  value of each independent triplicate study were plotted against the concentration of the [SAM]/ $K_m$ .

### Selectivity Studies

To determine selectivity, kinetic analysis of the peptide inhibitors was initially carried out using the SAH hydrolase-coupled fluorescence assay against G9a and PRMT1, respectively. The inhibitors were added at concentrations ranging from 0 to 100  $\mu\text{M}$  following a three-fold dilution. For G9a, the assay was performed in 1x PBS, pH7.4, 100  $\mu\text{M}$  SAM, 10  $\mu\text{M}$  SAH hydrolase, 25 nM G9a, inhibitors (0 – 100  $\mu\text{M}$ ), 20  $\mu\text{M}$  H3–15 peptide, and 15  $\mu\text{M}$  Thioglo1. For PRMT1, the assay was carried out in 2.5 mM HEPES (pH 7.0), 25 mM NaCl, 25  $\mu\text{M}$  EDTA, 50  $\mu\text{M}$  TCEP, 100  $\mu\text{M}$  SAM, 10  $\mu\text{M}$  SAH hydrolase, 200 nM PRMT1, 100  $\mu\text{M}$  H4–12 peptide, and 15  $\mu\text{M}$  Thioglo1. Fluorescence intensity was monitored using a CLARIOstar microplate reader (Ex = 370 nm, Em=500 nm) at 37  $^{\circ}\text{C}$  for 15 min. The rates were fit to the

log[inhibitor] vs response model using least squares nonlinear regression through GraphPad Prism 7 software. All experiments were performed in triplicate.

### Co-crystallization and Structure Determination

Purified NTMT1 at 30mg/ml was mixed with BM30 at a molar ratio of 1:2, incubated for 1 hr at 4°C. Broad matrix crystallization screening was performed using a Mosquito-LCP high throughput crystallization robot (TTP LabTech) using hanging-drop vapor diffusion method at 20°C. Crystals containing BM30 were grown in 0.1 M Na-HEPES, pH 7.5, 1.6 M ammonium sulfate, and 2% PEG 1000; all crystals were harvested directly from the drop and flash cooled into liquid nitrogen. Data were collected on single crystals at 12.0 keV at the GM/CA-CAT ID-D beamline at the Advanced Photon Source, Argonne National Laboratory. The data were processed using the on-site automated pipeline with Fast DP and molecular replacement performed with Phaser-MR (PHENIX).<sup>32,33</sup> All model building was performed using COOT and subsequent refinement done using phenix.refine (PHENIX).<sup>33,34</sup> The structure has been solved, refined and deposited into the Protein Data Bank with ID: 6WH8. Structure-related figures were made with PyMOL (Schrödinger) and annotated and finalized with Adobe Photoshop and Illustrator.

### In Vitro Methylation Assays with Full-length Recombinant Protein

All methylation assays were conducted at 30°C for 1 hour in methyltransferase buffer (50 mM potassium acetate, 50 mM Tris, pH 8.0). Recombinant NTMT1 (1 µg) was mixed with 1.0 µg full-length recombinant RCC1 and 100 µM SAM and inhibitors added to give the indicated concentrations (2, 10, and 50 µM). All His<sup>6</sup>-tagged recombinant proteins were expressed in *E. coli* and purified as previously described. The same batches of NTMT1 and RCC1 were used in all experiments. Positive controls contained no inhibitor, negative controls contained no NTMT1. One tenth of each reaction was mixed with 5x loading dye and loaded onto a 10% SDS-PAGE gel. Gels were transferred to nitrocellulose membranes using a Biorad Trans-Blot SD Semi-Dry Transfer Cell. Membranes were blocked for 1 h in 5% milk/TBST, then incubated with anti-me3-SPK (1:10,000), anti-me2-SPK (1:5000), or NTMT1 (1:1000) antibodies (add Tooley CE et al Nature 2010) overnight at 4 °C. They were then washed three times with 1x TBST and incubated with Rabbit IgG-HRP antibody (Jackson ImmunoResearch) for 1 h at room temperature. The membrane was washed three times with 1x TBST and detected using a Biorad ChemiDoc imaging system. Image quantification was done using ImageJ software (NIH). For Me3RCC1, all bands were compared to the untreated control, which was set at 1.0. For Me2RCC1, all bands were compared to the highest intensity band, which was set at 1.0. For NTMT1 and RCC1 loading controls, all bands were compared to the average band intensity, which was set at 1.0.

### Isothermal Titration Calorimetry

Isothermal titration calorimetry (ITC) measurements were performed at 25 °C by VP-ITC MicroCal calorimeter. Purified NTMT1 and NTMT2 were diluted with the ITC buffer (20 mM Tris-HCl pH 7.5, 150 mM NaCl and 0.5 mM TECP) to the final concentration of 30–50 µM, and the compounds were dissolved to 0.5–1mM in the same buffer. The compound was titrated into the protein solution with 26 injections of 10 µl each. Injections were spaced 180

sec with a reference power of 15  $\mu$ cal/sec. The ITC data were processed with Origin 7.0 software (Microcal).

### Cell Permeability Evaluation by MALDI

The colon cancer cell line HCT116 was cultured in McCoy's media supplemented with 10% fetal bovine serum and 1% Antibiotic-Antimycotic. The cells were cultured in tissue culture dish (Falcon 353003). Cells were maintained in cell culture flasks until seeding into a 24-well tissue culture plate (Falcon 353047). Media was removed and the cells were washed with 1xPBS (1 mL) twice followed by treating with TrypLE Express (1 mL) into a 100  $\times$  20 mm culture flask. The reaction was quenched by addition of 4 mL of media and the cells were counted. Cells were seeded into a 24-well tissue culture plate (Falcon 353047) at a density of  $0.1 \times 10^6$  cells/mL and incubated overnight at 37  $^{\circ}$ C, 5% CO<sub>2</sub>, and 95% humidity, with the lid on. They were then treated with the inhibitors at different concentrations and incubation was continued for the specified time. TAT peptide (GRKKRRQRRR-NH<sub>2</sub>) was also incubated as a control experiment. The media was removed, and the cells were washed with 1x PBS three times to remove any residual compound or peptide attached to the cell surface. Then 100  $\mu$ L of 1 x PBS was added and the cells were snap freeze in liquid nitrogen twice. The cell lysate was then analyzed with MALDI using DHB matrix to identify the presence of the compound inside the cell.

### Cellular N-methylation Level

HCT116 cells were seeded 20,000 cells/well on 24-well plates in the presence of 1x PBS or DC432 at different concentrations for 3 days. Then cells were lysed in 1x RIPA cell lysis buffer (25mM Tris-HCl pH 7.6, 150 mM NaCl, 1% NP-40, 1% sodium deoxycholate, 0.1% SDS, protease inhibitors) and incubated for 30 min on ice. The cell lysates were centrifuged at 15000 rpm for 10 min and the precipitates were removed. The concentration of total protein was quantified by bicinchoninic acid (BCA) protein assay kit (ThermoFisher, #23228). Equal amounts of total protein were mixed with 4x loading dye and loaded onto a 12.5% SDS-PAGE gel and separated. The gel was transferred to a polyvinylidene difluoride (PVDF) membrane using Biorad Trans-Blot Turbo system. The membrane was then blocked for 1 h in 5% milk TBST solution and washed with 1x TBST solution three times. The membrane was incubated with anti-me3-SPK antibody (1:5000), Lamin B1 antibody (1:2000), SET (1:1000) and RCC1 antibody (1:1000) at 4  $^{\circ}$ C for 12 h, washed with 1x TBST solution three times and then incubated with Rabbit IgG-HRP antibody (1:1000) for 1 h at room temperature. The membrane was again washed with 1x TBST solution three times and detected using a Protein Simple FluorChem imaging system. The data was analyzed in GraphPad prism software.

### Supplementary Material

Refer to Web version on PubMed Central for supplementary material.

### ACKNOWLEDGMENT

The authors acknowledge the support from NIH grants R01GM117275 (RH), 1R01GM127896 (NN), 1R01AI127793 (NN), R01GM112721 (CST), P30 CA023168 (Purdue University Center for Cancer Research), and

Natural Sciences and Engineering Research Council Grant RGPIN-2016-06300 (JM). The SGC is a registered charity (number 1097737) that receives funds from AbbVie, Bayer Pharma AG, Boehringer Ingelheim, Canada Foundation for Innovation, Eshelman Institute for Innovation, Genome Canada through Ontario Genomics Institute [OGI-055], Innovative Medicines Initiative (EU/EFPIA) [ULTRA-DD grant no. 115766], Janssen, Merck KGaA, Darmstadt, Germany, MSD, Novartis Pharma AG, Ontario Ministry of Research, Innovation and Science (MRIS), Pfizer, São Paulo Research Foundation-FAPESP, Takeda, and Wellcome. GM/CA@APS has been funded in whole or in part with Federal funds from the National Cancer Institute (ACB-12002) and the National Institute of General Medical Sciences (AGM-12006). This research used resources of the Advanced Photon Source, a U.S. Department of Energy (DOE) Office of Science User Facility operated for the DOE Office of Science by Argonne National Laboratory under Contract No. DE-AC02-06CH11357. We also thank supports from the Department of Medicinal Chemistry and Molecular Pharmacology (RH) and Department of Biological Sciences (NN) at Purdue University.

## ABBREVIATIONS

<b>NTMT</b>	protein N-terminal methyltransferase
<b>SAM</b>	S-5'-adenosyl-L-methionine
<b>SAH</b>	S-5'-adenosyl-L-homocysteines
<b>SAHH</b>	SAH hydrolase
<b>PKMT</b>	protein lysine methyltransferase
<b>PRMT</b>	protein arginine methyltransferase
<b>rt</b>	room temperature
<b>TFA</b>	trifluoroacetic acid

## REFERENCES

- (1). Ribich S; Harvey D; Copeland RA Review Drug Discovery and Chemical Biology of Cancer Epigenetics. *Cell Chem. Biol.* 2017, 24, 1120–1147. [PubMed: 28938089]
- (2). Scheer S; Ackloo S; Medina TS; Schapira M; Li F; Ward JA; Lewis AM; Northrop JP; Richardson PL; Kaniskan HÜ; Shen Y; Liu J; Smil D; McLeod D; Zepeda-Velazquez CA; Luo M; Jin J; Barsyte-Lovejoy D; Huber KVM; De Carvalho DD; Vedadi M; Zaph C; Brown PJ; Arrowsmith CH A Chemical Biology Toolbox to Study Protein Methyltransferases and Epigenetic Signaling. *Nat. Commun.* 2019, 10, 1–14. [PubMed: 30602773]
- (3). Chan-Penebre E; Kuplast KG; Majer CR; Boriack-Sjodin PA; Wigle TJ; Johnston LD; Rioux N; Munchhof MJ; Jin L; Jacques SL; West KA; Lingaraj T; Stickland K; Ribich SA; Raimondi A; Scott MP; Waters NJ; Pollock RM; Smith JJ; Barbash O; Pappalardi M; Ho TF; Nurse K; Oza KP; Gallagher KT; Kruger R; Moyer MP; Copeland RA; Chesworth R; Duncan KW A Selective Inhibitor of PRMT5 with in Vivo and in Vitro Potency in MCL Models. *Nat. Chem. Biol.* 2015, 11, 432–437. [PubMed: 25915199]
- (4). Huang R Chemical Biology of Protein N-Terminal Methyltransferases. *ChemBioChem* 2019, 20, 976–984. [PubMed: 30479015]
- (5). Chen R; Brosius J; Wittmann-Liebold B Occurrence of Methylated Amino Acids as N-Termini of Proteins from Escherichia Coli Ribosomes. *J. Mol. Biol.* 1977, 111, 173–181. [PubMed: 323502]
- (6). Schaner Tooley CE; Petkowski JJ; Muratore-Schroeder TL; Balsbaugh JL; Shabanowitz J; Sabat M; Minor W; Hunt DF; Macara IG NRMT Is an Alpha-N-Methyltransferase That Methylates RCC1 and Retinoblastoma Protein. *Nature* 2010, 466, 1125–1128. [PubMed: 20668449]
- (7). Webb KJ; Lipson RS; Al-Hadid Q; Whitelegge JP; Clarke SG Identification of Protein N-Terminal Methyltransferases in Yeast and Humans. *Biochemistry* 2010, 49, 5225–5235. [PubMed: 20481588]

- (8). Petkowski JJ; Bonsignore LA; Tooley JG; Wilkey DW; Merchant ML; Macara IG; Schaner Tooley CE NRMT2 Is an N-Terminal Monomethylase That Primes for Its Homologue NRMT1. *Biochem. J.* 2013, 456, 453–462. [PubMed: 24090352]
- (9). Dong C; Mao Y; Tempel W; Qin S; Li L; Loppnau P; Huang R; Min J Structural Basis for Substrate Recognition by the Human N-Terminal Methyltransferase 1. *Genes Dev.* 2015, 29, 2343–2348. [PubMed: 26543161]
- (10). Wu R; Yue Y; Zheng X; Li H Molecular Basis for Histone N-Terminal Methylation by NRMT1. *Genes Dev.* 2015, 29, 2337–2342. [PubMed: 26543159]
- (11). Dong C; Dong G; Li L; Zhu L; Tempel W; Liu Y; Huang R; Min J An Asparagine/Glycine Switch Governs Product Specificity of Human N-Terminal Methyltransferase NTMT2. *Commun. Biol* 2018, 1, 183. [PubMed: 30417120]
- (12). Jakobsson ME; Matecki JM; Halabelian L; Nilges BS; Pinto R; Kudithipudi S; Munk S; Davydova E; Zuhairi FR; Arrowsmith CH; Jeltsch A; Leidel SA; Olsen JV; Falnes PØ The Dual Methyltransferase METTL13 Targets N Terminus and Lys55 of EEF1A and Modulates Codon-Specific Translation Rates. *Nat. Commun.* 2018, 9, 3411. [PubMed: 30143613]
- (13). Liu S; Hausmann S; Carlson SM; Fuentes ME; Francis JW; Pillai R; Lofgren SM; Hulea L; Tandoc K; Lu J; Li A; Nguyen ND; Caporicci M; Kim MP; Maitra A; Wang H; Wistuba II; Porco JA Jr.; Bassik MC; Elias JE; Song J; Topisirovic I; Van Rechem C; Mazur PK; Gozani O METTL13 Methylation of EEF1A Increases Translational Output to Promote Tumorigenesis. *Cell* 2019, 176, 491–504.e21. [PubMed: 30612740]
- (14). Nomoto Minoru, Kyogoku Yoshimasa, and K. I. N-Trimethylalanine, a Novel Blocked N-Terminal Residue of Tetrahymena Histone H2B. *J. Biochem* 1982, 92, 1675–1678. [PubMed: 6818230]
- (15). Sathyan KM; Fachinetti D; Foltz DR  $\alpha$ -Amino Trimethylation of CENP-A by NRMT Is Required for Full Recruitment of the Centromere. *Nat. Commun.* 2017, 8, 14678. [PubMed: 28266506]
- (16). Chen T; Muratore TL; Schaner Tooley CE; Shabanowitz J; Hunt DF; Macara IG N-Terminal Alpha-Methylation of RCC1 Is Necessary for Stable Chromatin Association and Normal Mitosis. *Nat. Cell Biol.* 2007, 9, 596–603. [PubMed: 17435751]
- (17). Cai Q; Fu L; Wang Z; Gan N; Dai X; Wang Y  $\alpha$ -N-Methylation of Damaged DNA-Binding Protein 2 (DDB2) and Its Function in Nucleotide Excision Repair. *J. Biol. Chem.* 2014, 289, 16046–16056. [PubMed: 24753253]
- (18). Dai X; Rulten SL; You C; Caldecott KW; Wang Y Identification and Functional Characterizations of N-Terminal Alpha-N-Methylation and Phosphorylation of Serine 461 in Human Poly(ADP-ribose) Polymerase 3. *J Proteome Res* 2015, 14, 2575–2582. [PubMed: 25886813]
- (19). Shields KM; Tooley JG; Petkowski JJ; Wilkey DW; Garbett NC; Merchant ML; Cheng A; Schaner Tooley CE Select Human Cancer Mutants of NRMT1 Alter Its Catalytic Activity and Decrease N-Terminal Trimethylation. *Protein Sci.* 2017, 26, 1639–1652. [PubMed: 28556566]
- (20). Bonsignore LA; Tooley JG; Van Hoose PM; Wang E; Cheng A; Cole MP; Schaner Tooley CE NRMT1 Knockout Mice Exhibit Phenotypes Associated with Impaired DNA Repair and Premature Aging. *Mech. Ageing Dev.* 2015, 146, 42–52. [PubMed: 25843235]
- (21). Hitakomate E; Hood FE; Sanderson HS; Clarke PR The Methylated N-Terminal Tail of RCC1 Is Required for Stabilisation of Its Interaction with Chromatin by Ran in Live Cells. *BMC Cell Biol.* 2010, 11, 43. [PubMed: 20565941]
- (22). Richardson SL; Mao Y; Zhang G; Hanjra P; Peterson DL; Huang R Kinetic Mechanism of Protein N-Terminal Methyltransferase 1. *J. Biol. Chem.* 2015, 290, 11601–11610. [PubMed: 25771539]
- (23). Zhang G; Richardson SL; Mao Y; Huang R Design, Synthesis, and Kinetic Analysis of Potent Protein N-Terminal Methyltransferase 1 Inhibitors. *Org. Biomol. Chem.* 2015, 13, 4149–4154. [PubMed: 25712161]
- (24). Zhang G; Huang R Facile Synthesis of SAM-Peptide Conjugates through Alkyl Linkers Targeting Protein N-Terminal Methyltransferase 1. *RSC Adv.* 2016, 6, 6768–6771. [PubMed: 27588169]

- (25). Chen D; Dong G; Noinaj N; Huang R Discovery of Bisubstrate Inhibitors for Protein N-Terminal Methyltransferase 1. *J. Med. Chem.* 2019, 62, 3773–3779. [PubMed: 30883119]
- (26). Chen D; Dong C; Dong G; Srinivasan K; Min J; Noinaj N; Huang R Probing the Plasticity in the Active Site of Protein N-Terminal Methyltransferase 1 Using Bisubstrate Analogs. *J. Med. Chem.* 2020, 63, 8419–8431. 10.1021/acs.jmedchem.0c00770 [PubMed: 32605369]
- (27). Petkowski JJ; Schaner Tooley CE; Anderson LC; Shumilin IA; Balsbaugh JL; Shabanowitz J; Hunt DF; Minor W; Macara IG Substrate Specificity of Mammalian N-Terminal  $\alpha$ -Amino Methyltransferase. *Biochemistry* 2012, 51, 5942–5950. [PubMed: 22769851]
- (28). Richardson SL; Hanjra P; Zhang G; Mackie BD; Peterson DL; Huang R A Direct, Ratiometric, and Quantitative MALDI-MS Assay for Protein Methyltransferases and Acetyltransferases. *Anal. Biochem.* 2015, 478, 59–64. [PubMed: 25778392]
- (29). De Poli M; Moretto A; Crisma M; Peggion C; Formaggio F; Kaptein B; Broxterman QB; Toniolo C Is the Backbone Conformation of C $\alpha$ -Methyl Proline Restricted to a Single Region? *Chem. - A Eur. J* 2009, 15, 8015–8025.
- (30). Chen D; Li L; Diaz K; Iyamu ID; Yadav R; Noinaj N; Huang R Novel Propargyl-Linked Bisubstrate Analogues as Tight-Binding Inhibitors for Nicotinamide N-Methyltransferase. *J. Med. Chem.* 2019, 62, 10783–10797. [PubMed: 31724854]
- (31). Qian Z; Liu T; Liu Y-YY; Briesewitz R; Barrios AM; Jhiang SM; Pei D Efficient Delivery of Cyclic Peptides into Mammalian Cells with Short Sequence Motifs. *ACS Chem. Biol.* 2013, 8, 423–431. [PubMed: 23130658]
- (32). Winter G; Ashton A Fast\_dp. *Methods Zenodo.* 2014, 55, 81–93.
- (33). Adams PD; Afonine PV; Bunkóczi G; Chen VB; Davis IW; Echols N; Headd JJ; Hung LW; Kapral GJ; Grosse-Kunstleve RW; McCoy AJ; Moriarty NW; Oeffner R; Read RJ; Richardson DC; Richardson JS; Terwilliger TC; Zwart PH PHENIX: A Comprehensive Python-Based System for Macromolecular Structure Solution. *Acta Crystallogr. Sect. D Biol. Crystallogr.* 2010, 66, 213–221. [PubMed: 20124702]
- (34). Emsley P; Lohkamp B; Scott WG; Cowtan K Features and Development of Coot. *Acta Crystallogr., Sect. D: Biol. Crystallogr.* 2010, 66, 486–501. [PubMed: 20383002]

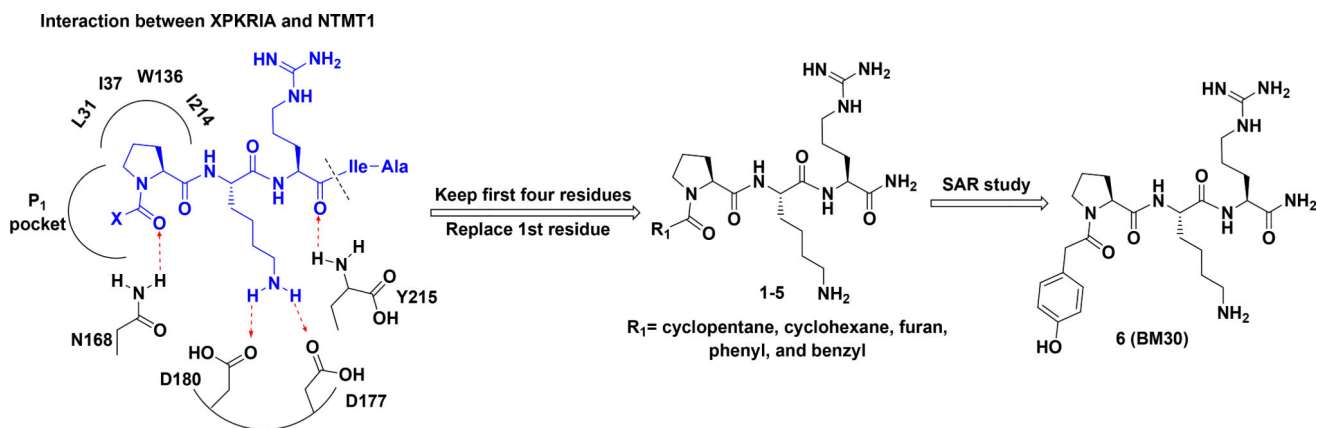


**Figure 1.** Design inhibitors based on the structure of NTMT1 peptide substrates. H-bond interactions are shown in red dotted lines.

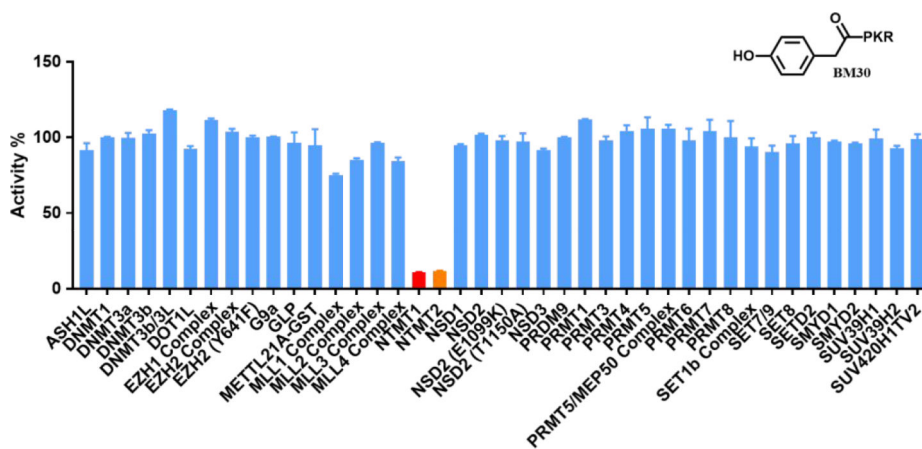


**Figure 2.** Selectivity of NTMT inhibitor **BM30**. Selectivity of **BM30** against a panel of 41 PKMTs, PRMTs, DNMTs and NTMT1/2 was determined at concentration of 100  $\mu$ M in duplicates (n=2).



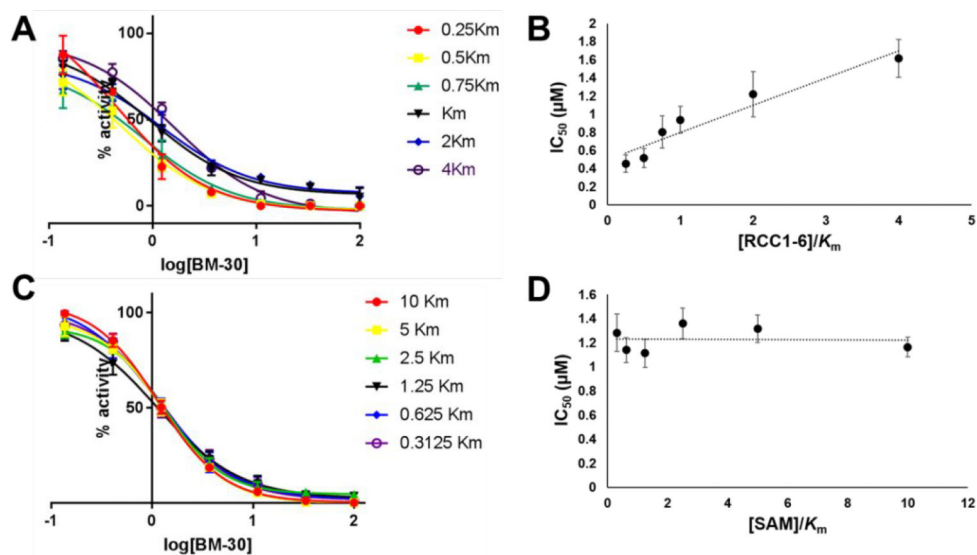


**Figure 3.**

Inhibition mechanism of **BM30**. All experiments were run in triplicate (n=3). (A) IC<sub>50</sub> curves of **BM30** at varying concentrations of NTMT1 peptide substrate, RCC1-6 (SPKRIA), with fixed concentration of SAM; (B) linear regression plot of IC<sub>50</sub> values with corresponding concentrations of RCC1-6; (C) IC<sub>50</sub> curves of **BM30** at varying concentrations of SAM with fixed concentration of RCC1-6; (D) Plot of IC<sub>50</sub> values with corresponding concentrations of SAM.

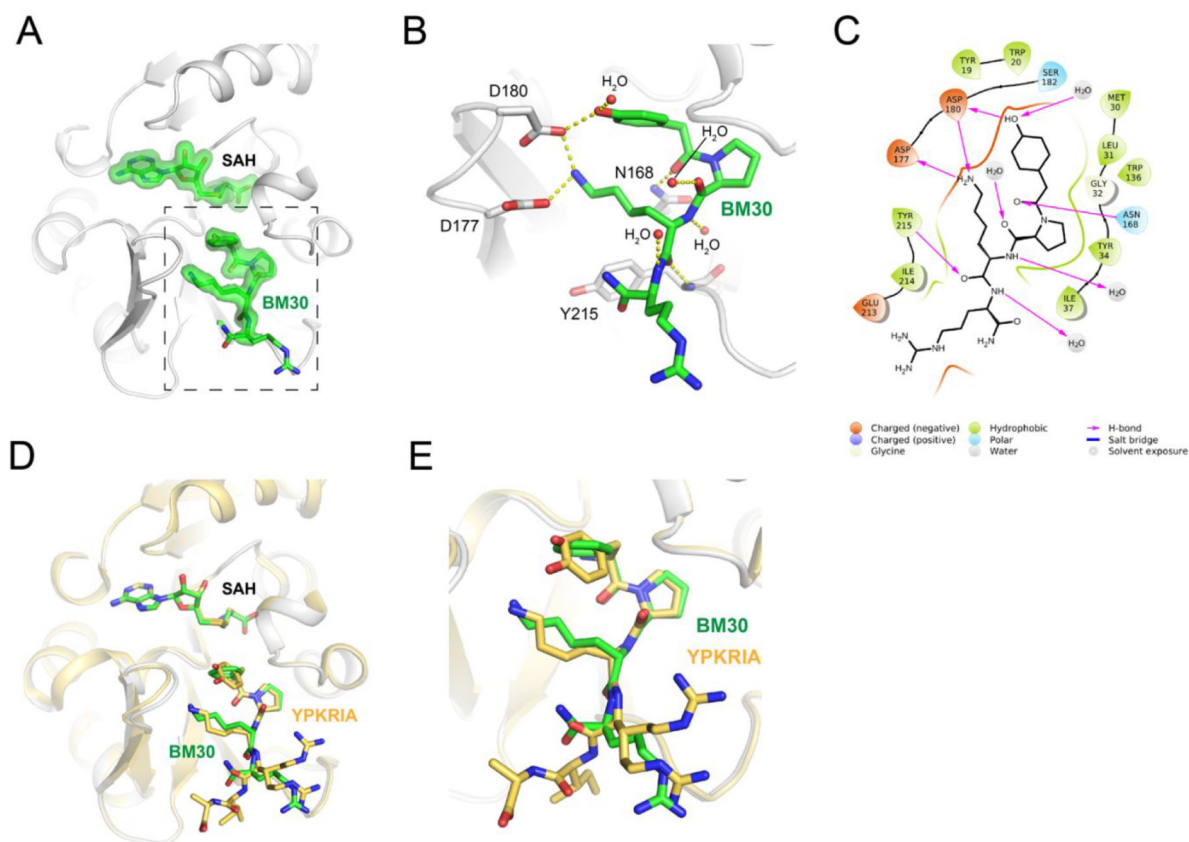


**Figure 4.** Co-crystal structure of NTMT1(gray cartoon)-**BM30** (green stick)-SAH (green stick) (PDB ID: 6WH8). (A) Fo-Fc omit density map of ligands. (B) Zoomed view of interactions of **BM30** with NTMT1. H-bond interactions are shown in yellow dotted lines. (C) **BM30** interaction diagram (Schrödinger Maestro) with NTMT1. (D) and (E) Structural alignment of NTMT1(gray)-**BM30** (green stick)-SAH (green stick) and NTMT1(yellow cartoon)-YPKRIA (yellow stick)-SAH (yellow stick) (PDB ID: 5E1D)

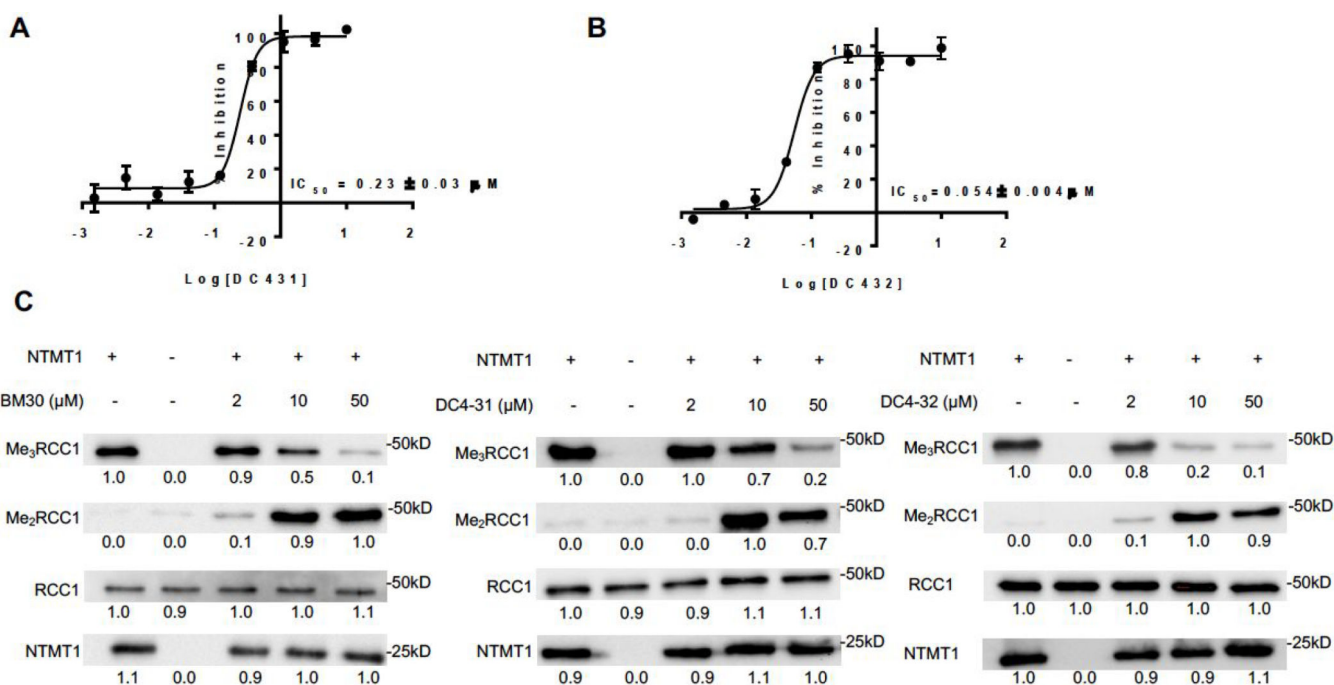


**Figure 5.** Biochemical characterization of **DC431** and **DC432**. (A,B) IC<sub>50</sub> curve of **DC431** and **DC432**. IC<sub>50</sub> values were determined in triplicates (n = 3) and presented as mean ± SD. (C) Representative western blots showing N-terminal dimethylation (Me<sub>2</sub>RCC1) and trimethylation (Me<sub>3</sub>RCC1) of full-length recombinant human RCC1 by full-length recombinant human NTMT1 in the presence of increasing concentrations of **BM30**, **DC431** and **DC432** (n=3). NTMT1 and RCC1 blots are shown as loading controls.

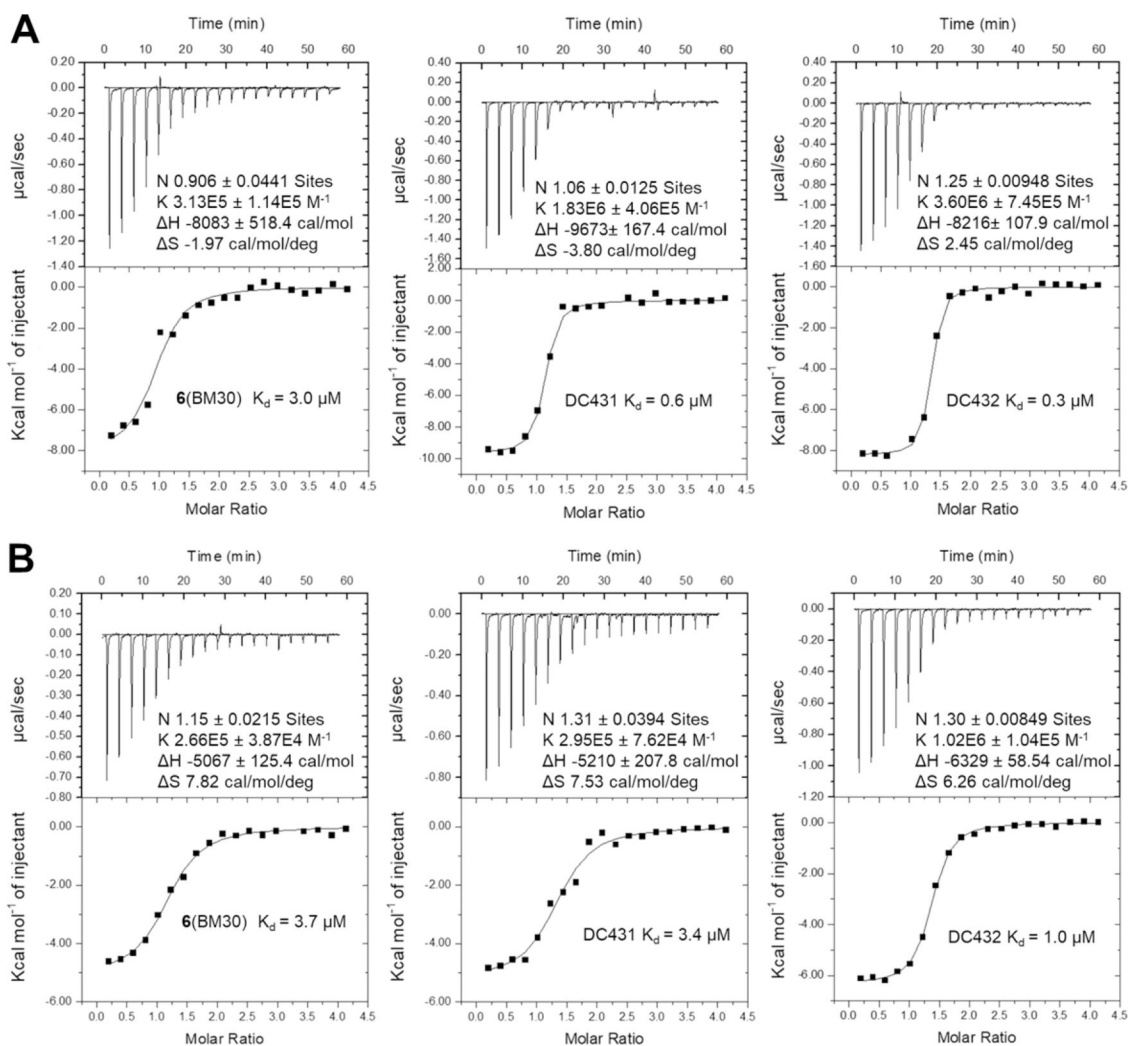


**Figure 6.**  
Binding affinity for NTMT1(A) (n=2) and NTMT2 (B) (n=1).

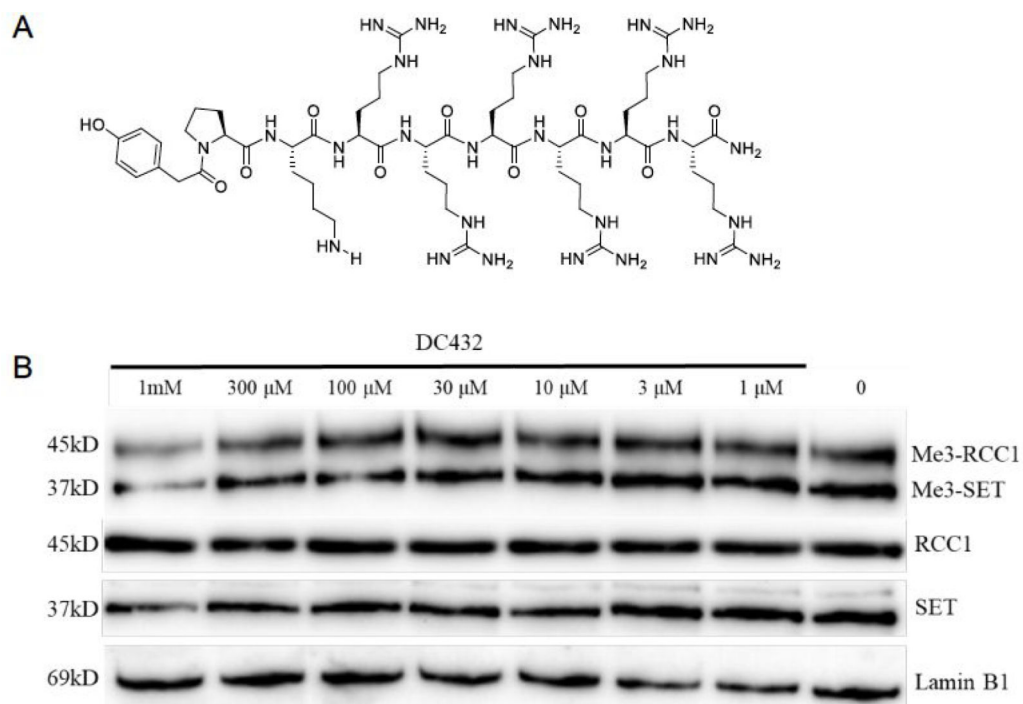


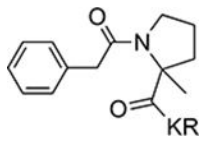
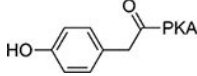
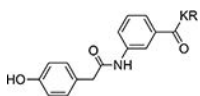
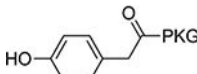
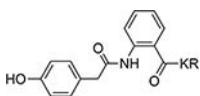
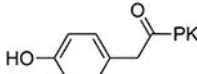
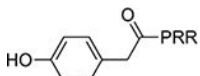
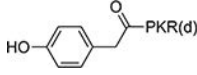
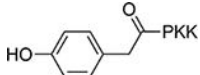
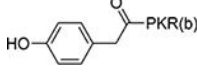
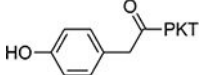
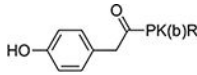
**Figure 7.** Cellular N-terminal methylation assay of compound DC432 in HCT116 cells. (A) Structure of DC432. (B) Representative western blot results of effects of DC432 (0–1 mM) on cellular methylation level (n=2). RCC1, SET, and Lamin B1 blots are shown as loading controls.

**Table 1.**SAR of the first position of R<sub>1</sub>-PKR\*

Compound	Structure	IC <sub>50</sub> (μM)	Compound	Structure	IC <sub>50</sub> (μM)
1		>100	7		4.3±0.28
2		>100	8		>100
3		>100	9		1.5±0.1
4		>100	10		4.5±0.5
5		6.85±2.82	11		12±1.4
6 (BM30)		0.89±0.10	12		>100

\*IC<sub>50</sub> values were determined in triplicates (n = 3) and presented as mean ± standard deviation (SD).

**Table 2.**SAR of the 2<sup>nd</sup>-4<sup>th</sup> position of R<sub>1</sub>-PKR\*

Compound	Structure	IC <sub>50</sub> (μM)	Compound	Structure	IC <sub>50</sub> (μM)
13		>100	19		4.8±0.71
14		>100	20		13±1.6
15		>100	21		16±4.7
16		21±3.3	22		4.2±1.2
17		1.0±0.22	23		6.4±0.5
18		4.8±0.31	24		32.9±8.3

\*IC<sub>50</sub> values were determined in triplicates (n = 3) and presented as mean ± SD.